# Supplementary Material

# Mineralogy and physicochemical features of Saharan dust wet deposited in the Iberian Peninsula during an extreme red rain event

Carlos Rodriguez-Navarro, Fulvio di Lorenzo, and Kerstin Elert

Department Dept. Mineralogy and Petrology, University of Granada, Fuentenueva s/n, 18002 Granada, Spain

*Correspondence to*: Carlos Rodriguez-Navarro (carlosrn@ugr.es)

**Content**

**Table S1. Structural formulae of clay minerals (all analyses) in Saharan dust from TEM-AEM analysis**

| | Si | $Al^{IV}$ | $Al^{VI}$ | Mg | Fe | Sum Oct[1] | K | Ca | Na | Sum Int.[2] |
|---|---|---|---|---|---|---|---|---|---|---|
| Illite based on $O_{10}(OH)_2$ | | | | | | | | | | |
| 1 | 3.53 | 0.47 | 1.69 | 0.19 | 0.14 | 2.03 | 0.58 | 0.00 | 0.00 | 0.58 |
| 2 | 3.39 | 0.61 | 1.29 | 0.20 | 0.60 | 2.09 | 0.34 | 0.11 | 0.12 | 0.67 |
| 3 | 3.34 | 0.66 | 1.43 | 0.42 | 0.32 | 2.17 | 0.56 | 0.00 | 0.00 | 0.56 |
| 4 | 3.33 | 0.67 | 1.20 | 0.40 | 0.43 | 2.03 | 0.51 | 0.00 | 0.00 | 0.51 |
| 5 | 3.35 | 0.65 | 1.65 | 0.30 | 0.22 | 2.17 | 0.44 | 0.00 | 0.00 | 0.44 |
| Aver. | 3.46 | 0.54 | 1.49 | 0.20 | 0.37 | 2.06 | 0.46 | 0.06 | 0.06 | 0.63 |
| Std. | ±0.10 | ±0.10 | ±0.28 | ±0.01 | ±0.33 | ±0.04 | ±0.17 | ±0.08 | ±0.08 | ±0.06 |
| Palygorskite based on $O_{10}OH$ | | | | | | | | | | |
| 1 | 4.41 | 0.00 | 0.70 | 0.54 | 0.07 | 1.30 | 0.00 | 0.00 | 0.00 | |
| 2 | 3.85 | 0.00 | 0.98 | 0.34 | 0.59 | 1.92 | 0.12 | 0.03 | 0.00 | |
| 3 | 3.95 | 0.00 | 0.83 | 0.73 | 0.41 | 1.96 | 0.05 | 0.00 | 0.00 | |
| 4 | 4.11 | 0.00 | 0.82 | 0.57 | 0.28 | 1.67 | 0.05 | 0.05 | 0.00 | |
| 5 | 4.25 | 0.00 | 0.61 | 0.80 | 0.16 | 1.57 | 0.07 | 0.02 | 0.00 | |
| 6 | 4.22 | 0.00 | 0.35 | 1.33 | 0.12 | 1.79 | 0.07 | 0.00 | 0.00 | |
| 7 | 3.94 | 0.00 | 0.80 | 1.00 | 0.24 | 2.04 | 0.05 | 0.04 | 0.00 | |
| 8 | 4.22 | 0.00 | 0.55 | 1.34 | 0.18 | 2.07 | 0.00 | 0.06 | 0.00 | |
| Aver. | 4.08 | 0.00 | 0.63 | 1.10 | 0.24 | 1.97 | 0.04 | 0.03 | 0.00 | |
| Std. | ±0.17 | ±0.00 | ±0.25 | ±0.42 | ±0.19 | ±0.11 | ±0.04 | ±0.03 | ±0.00 | |
| Kaolinite based on $O_5(OH)_4$ | | | | | | | | | | |
| 1 | 2.02 | 0.00 | 1.82 | 0.00 | 0.15 | 0.00 | 0.00 | 0.00 | 0.00 | |
| 2 | 2.02 | 0.00 | 1.92 | 0.00 | 0.03 | 0.00 | 0.00 | 0.03 | 0.00 | |
| 3 | 2.01 | 0.00 | 1.98 | 0.00 | 0.02 | 0.00 | 0.00 | 0.00 | 0.00 | |
| 4 | 1.98 | 0.00 | 2.01 | 0.00 | 0.02 | 0.00 | 0.00 | 0.00 | 0.00 | |
| 5 | 2.01 | 0.00 | 1.87 | 0.07 | 0.06 | 0.00 | 0.00 | 0.01 | 0.00 | |
| 6 | 1.98 | 0.00 | 1.96 | 0.01 | 0.06 | 0.00 | 0.00 | 0.00 | 0.00 | |
| 7 | 2.05 | 0.00 | 1.82 | 0.00 | 0.88 | 0.00 | 0.00 | 0.00 | 0.00 | |
| Aver. | 2.01 | 0.00 | 1.91 | 0.01 | 0.06 | 0.00 | 0.00 | 0.01 | 0.00 | |
| Std. | ±0.02 | ±0.00 | ±0.08 | ±0.03 | ±0.05 | ±0.00 | ±0.00 | ±0.01 | ±0.00 | |
| Smectite based on $O_{10}(OH)_2$ | | | | | | | | | | |
| 1 | 4.01 | 0.00 | 1.54 | 0.09 | 0.26 | 1.89 | 0.14 | 0.14 | 0.00 | 0.42 |
| 2 | 3.62 | 0.38 | 1.21 | 0.31 | 0.56 | 2.08 | 0.21 | 0.12 | 0.00 | 0.45 |
| 3 | 3.71 | 0.29 | 1.32 | 0.19 | 0.52 | 2.03 | 0.16 | 0.12 | 0.00 | 0.40 |

| | | | | | | | | | | |
|---|---|---|---|---|---|---|---|---|---|---|
| 4 | 3.51 | 0.49 | 1.59 | 0.21 | 0.37 | 2.16 | 0.17 | 0.02 | 0.00 | 0.20 |
| 5 | 3.38 | 0.62 | 1.64 | 0.16 | 0.30 | 2.09 | 0.09 | 0.21 | 0.00 | 0.51 |
| 6 | 3.84 | 0.16 | 1.51 | 0.22 | 0.26 | 2.00 | 0.05 | 0.17 | 0.00 | 0.39 |
| 7 | 3.64 | 0.36 | 1.51 | 0.37 | 0.28 | 2.16 | 0.15 | 0.06 | 0.00 | 0.27 |
| 8 | 3.55 | 0.45 | 1.82 | 0.15 | 0.16 | 2.13 | 0.15 | 0.03 | 0.00 | 0.21 |
| 9 | 3.42 | 0.58 | 1.73 | 0.25 | 0.23 | 2.21 | 0.11 | 0.05 | 0.00 | 0.21 |
| 10 | 3.65 | 0.37 | 1.01 | 0.89 | 0.47 | 2.37 | 0.11 | 0.00 | 0.00 | 0.11 |
| Aver. | 3.58 | 0.42 | 1.54 | 0.23 | 0.34 | 2.11 | 0.14 | 0.10 | 0.00 | 0.33 |
| Std. | ±0.15 | ±0.15 | ±0.20 | ±0.08 | ±0.14 | ±0.07 | ±0.05 | ±0.07 | ±0.00 | ±0.12 |
| Illite-smectite mixed layer based on $O_{10}(OH)_2$ | | | | | | | | | | |
| 1 | 3.25 | 0.75 | 1.77 | 0.26 | 0.24 | 2.27 | 0.14 | 0.02 | 0.00 | 0.18 |
| 2 | 3.57 | 0.43 | 0.93 | 0.12 | 0.92 | 1.98 | 0.24 | 0.19 | 0.00 | 0.62 |
| 3 | 3.71 | 0.29 | 0.91 | 0.35 | 0.77 | 2.03 | 0.31 | 0.12 | 0.00 | 0.55 |
| 4 | 3.66 | 0.34 | 1.57 | 0.42 | 0.13 | 2.12 | 0.30 | 0.05 | 0.00 | 0.40 |
| Aver. | 3.46 | 0.54 | 1.67 | 0.34 | 0.19 | 2.20 | 0.22 | 0.04 | 0.00 | 0.29 |
| Std. | ±0.29 | ±0.29 | ±0.14 | ±0.11 | ±0.08 | ±0.11 | ±0.11 | ±0.02 | ±0.00 | ±0.16 |

[1] Sum of octahedral cations

[2] Sum of interlayer charge ($M^+ + M^{2+}$)

Structural formulae in red are not fully reliable (either due to too high or too low Sum oct., or excessive Fe -due to possible contamination with iron oxyhydroxide nanoparticles-). Therefore, they are not considered for the calculation of the average structural formulae.

**Table S2**. **Results of PHREEQC geochemical modeling of Saharan dust dissolution in rainwater (for an equilibrium pH = 8)**

| Phases | Molecular weight | SI | Initial amount (mol/L) | Amount dissolved (mol/L) | % dissolved |
|---|---|---|---|---|---|
| ferrihydrite | 106.866 | 0 | 7.58E-04 | 2.32E-06 | 0.31 |
| goethite | 88.851 | 5.3 | 1.71E-03 | 0 | 0 |
| hematite | 159.687 | 11.53 | 2.79E-04 | 0 | 0 |
| kaolinite | 258.155 | 3.3 | 2.27E-03 | 0 | 0 |
| quartz | 60.083 | 1.21 | 3.41E-02 | 0 | 0 |
| calcite | 100.086 | 0 | 1.07E-02 | 2.47E-04 | 2.3 |
| dolomite | 184.399 | 1.44 | 9.67E-04 | 0 | 0 |
| plagioclase (albite) | 278.202 | 2.1 | 2.24E-03 | 0 | 0 |
| illite | 383.893 | 2.3 | 5.13E-03 | 0 | 0 |
| k feldspar (microcline) | 278.326 | 0 | 1.92E-03 | 2.59E-08 | 0.001 |
| rutile | 79.865 | 0 | 8.93E-04 | 2.26E-10 | 2E-5 |
| smectite (high Mg-Fe) | 404.191 | 0 | 1.56E-03 | 3.99E-11 | 2.5E-6 |
| sepiolite (for palygorskite) | 647.819 | 0 | 2.45E-03 | 1.29E-04 | 5.2 |

**Note**: A value of SI = 0 means that the specific phase dissolved until equilibrium (saturation). Conversely, values of SI > 0 mean that the specific phase(s) is highly supersaturated and cannot dissolve.

**Table S3. Calculation of the total structural Fe in the clay minerals of the Saharan dust**

| | Fractional amount in bulk *From XRD results (Table 2)* | Fe (mol per formula unit) *Based on one Si/formula unit* | Fe in clays (wt%) | Fe in bulk dust (wt%) |
|---|---|---|---|---|
| Illite | 0.145 | 0.093 | 5.18 | 0.75 |
| palygorskite | 0.170 | 0.060 | 3.36 | 0.57 |
| smectite | 0.047 | 0.085 | 4.76 | 0.22 |
| kaolinite | 0.082 | 0.030 | 1.68 | 0.14 |
| MLC | 0.010 | 0.048 | 2.66 | 0.03 |
| Chlorite | 0.019 | 0.250 | 14.00 | 0.27 |
| | | | Average Fe in clays | Total structural Fe |
| | | | 5.27 | **1.98** |

**Note**: the content of structural iron in each clay was determined by: (1) calculating the fractional amount of each clay mineral in the bulk dust (from Table 2); (2) dividing the amount (in moles) of Fe determined by TEM-AEM analysis (structural formulae in Table 4) by the total moles of tetrahedral cations in the structural formula of each clay mineral; (3) the resulting value was multiplied by the atomic weight of Fe (56), yielding the Fe present (wt%) in each clay mineral ; (4) this later value was in turn multiplied by the fractional amount of each clay mineral, thereby yielding the contribution of each clay to the "Fe in bulk dust (wt%)", and the total structural Fe.

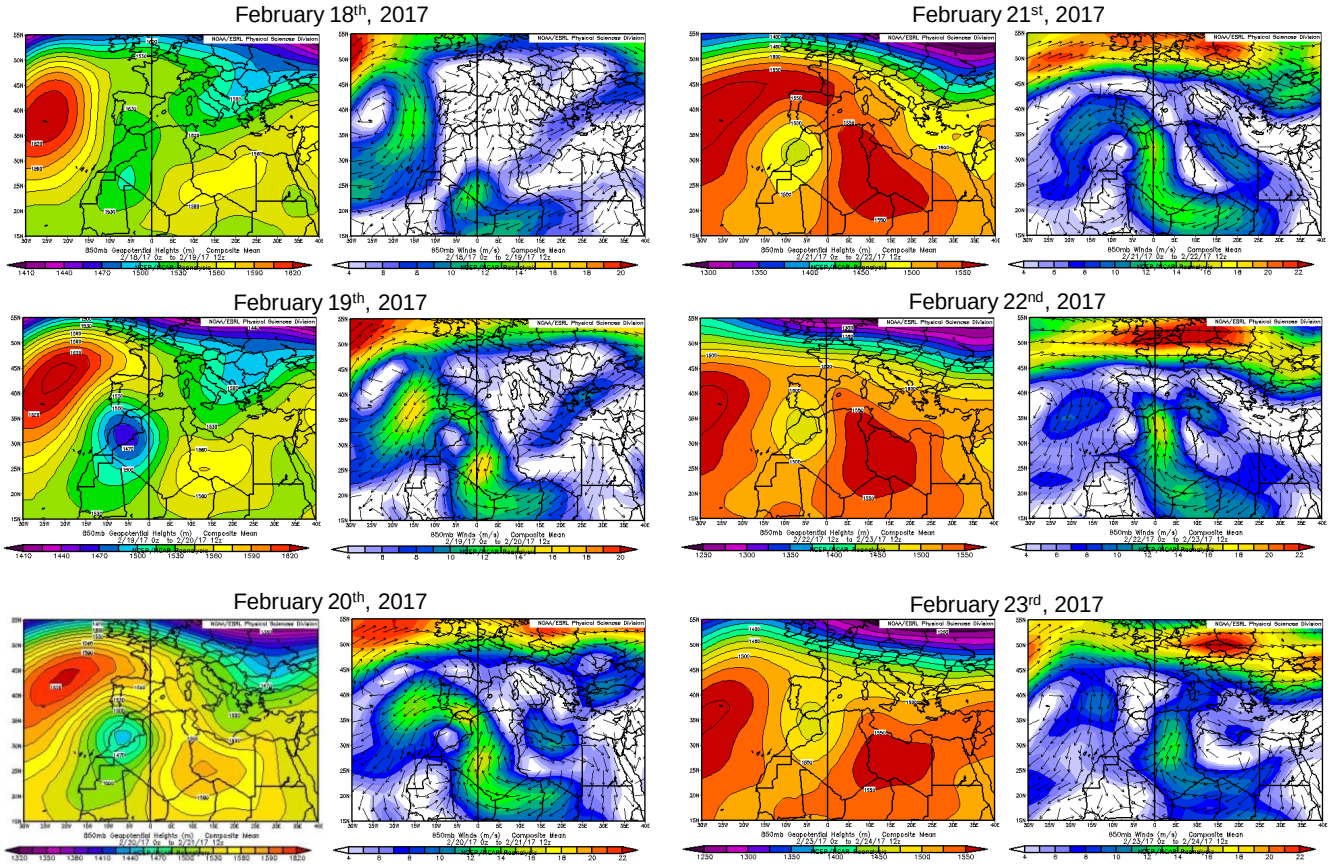


**Figure S1.** Daily synoptic scale meteorological situation during the days before, during and after the red rain event based on NOAA/ESRL reanalysis for 850 hPa geopotential height. For each date, paired maps of geopotential height and wind field are presented.

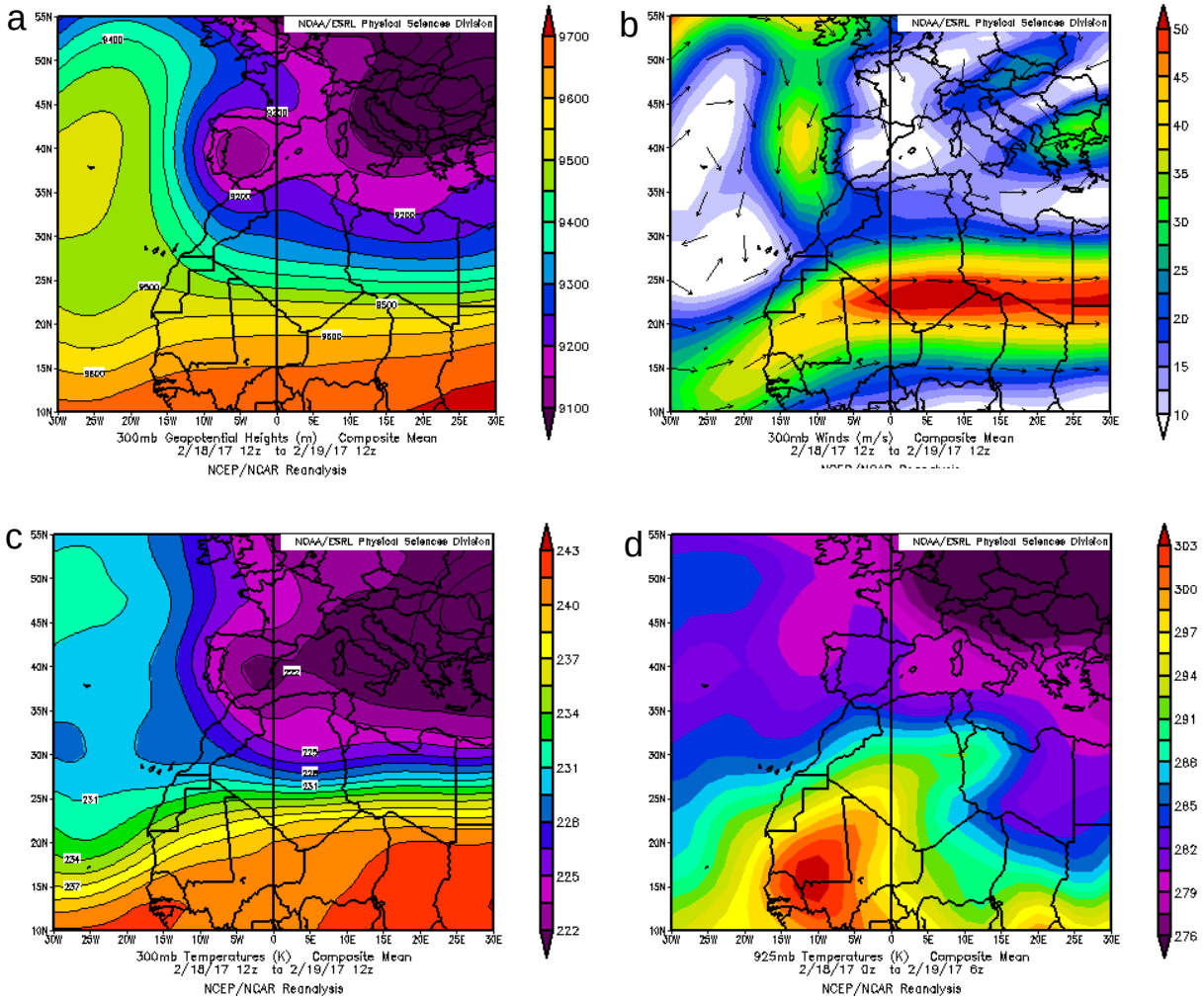


**Figure S2.** Synoptic scale meteorological situation during the days preceding the development of the north African cyclone responsible for the extreme red rain event (NOAA/ESRL reanalysis). Averaged geopotential heigth (a) and wind field (b), and temperature at 300 hPa (c) and at 925 hPa (d) during February 18-19, 2017.

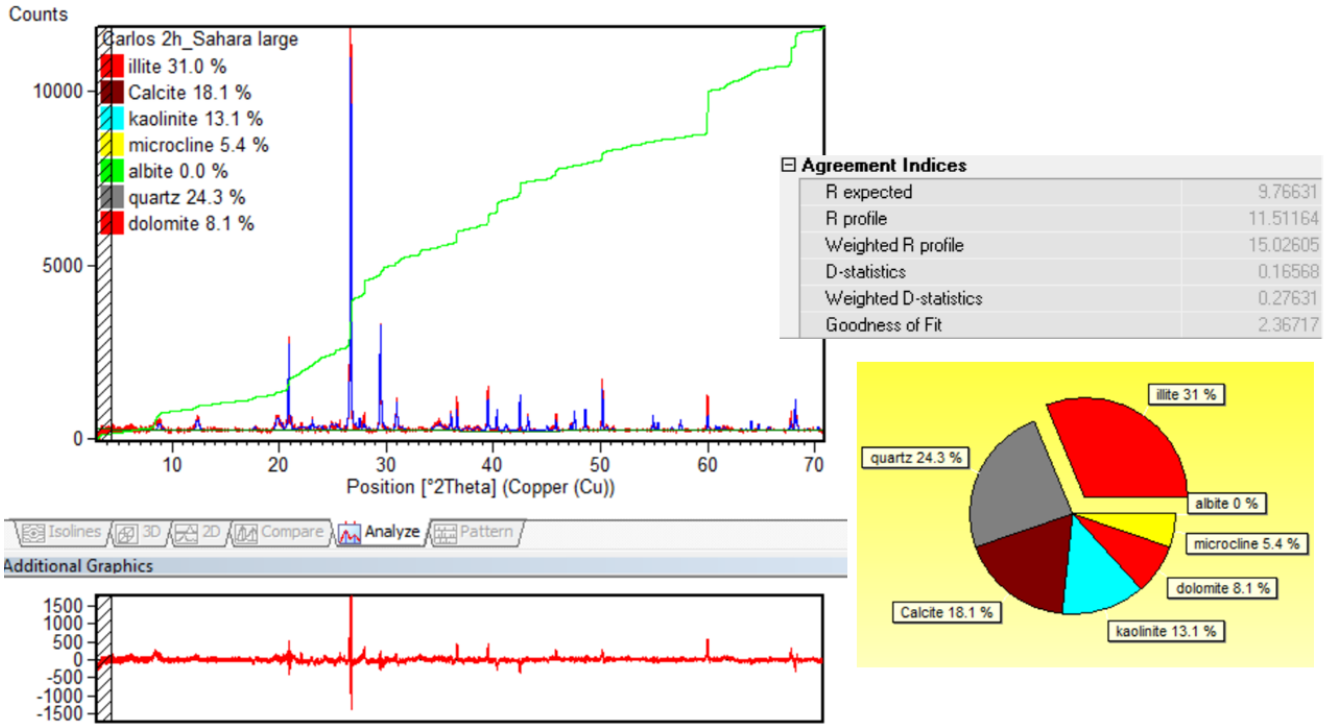


**Figure S3.** Semiquantitative XRD analysis of a Saharan dust sample collected during the extreme red rain event and performed using the Rietveld full pattern profile method. In addition to the experimental (red) and modeled (bleu) pattern profiles (upper left corner image), the residual curve is shown (lower left) as well as the results of the semiquantitaive analysis (graph on the right).

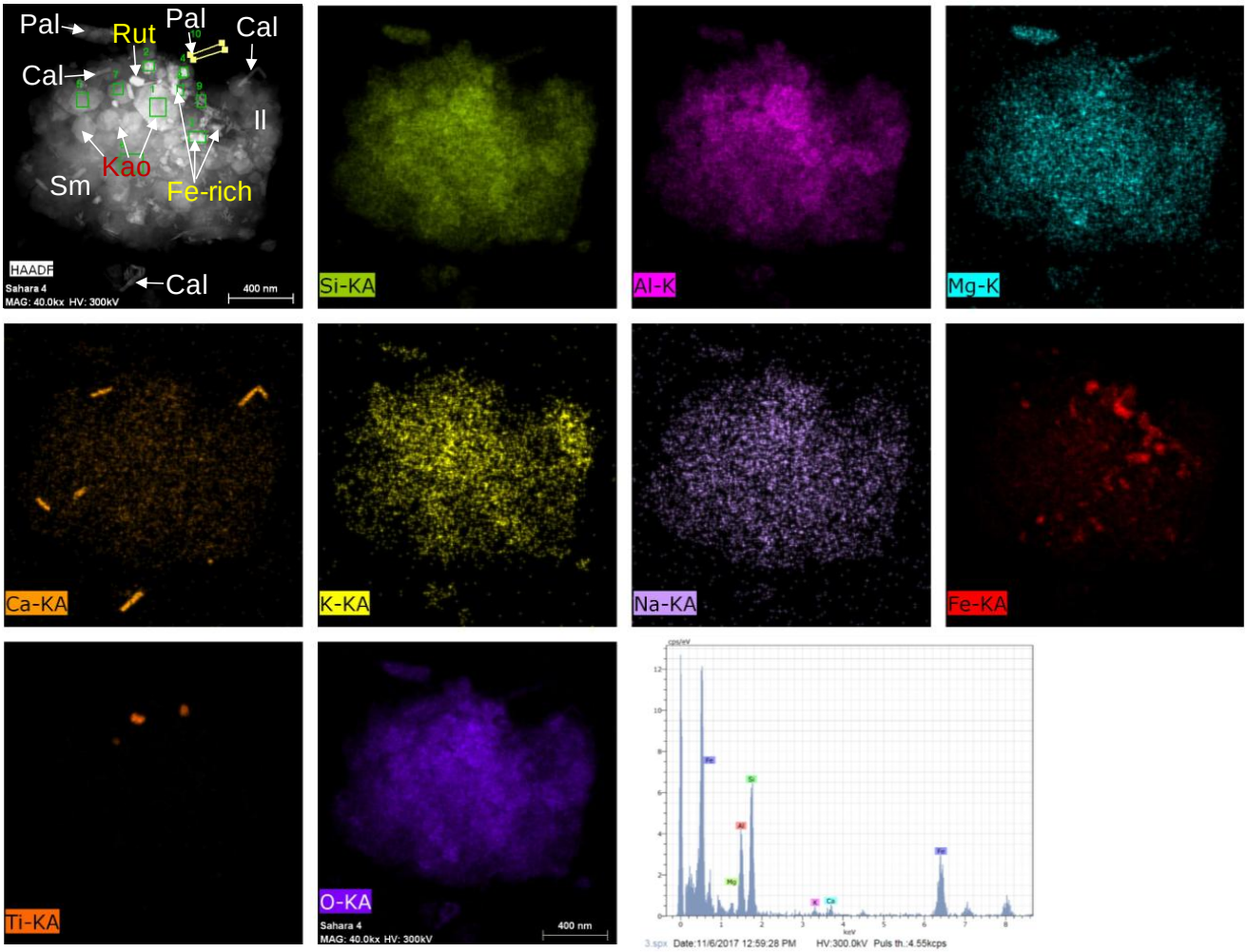


**Figure S4.** STEM-HAADF photomicrographs and corresponding EDX elemental maps of a clay-rich micrometer-sized aggregate of Saharan dust particles. Based on the compositional analysis, particles of palygorskite (Pal), calcite (Cal), aggregates of iron oxyhydroxide nanoparticle (Fe-rich), rutile (Rut), illite (Il), smectite (Sm), and kaolinite (Kao) were identified. The EDX spectrum corresponds to Fe-rich nanoparticles attached onto the clay minerals (analysis #3 in HAADF image). Note: analyzed spots are outlined with green or yellow (numbered) rectangles in the HAADF image.

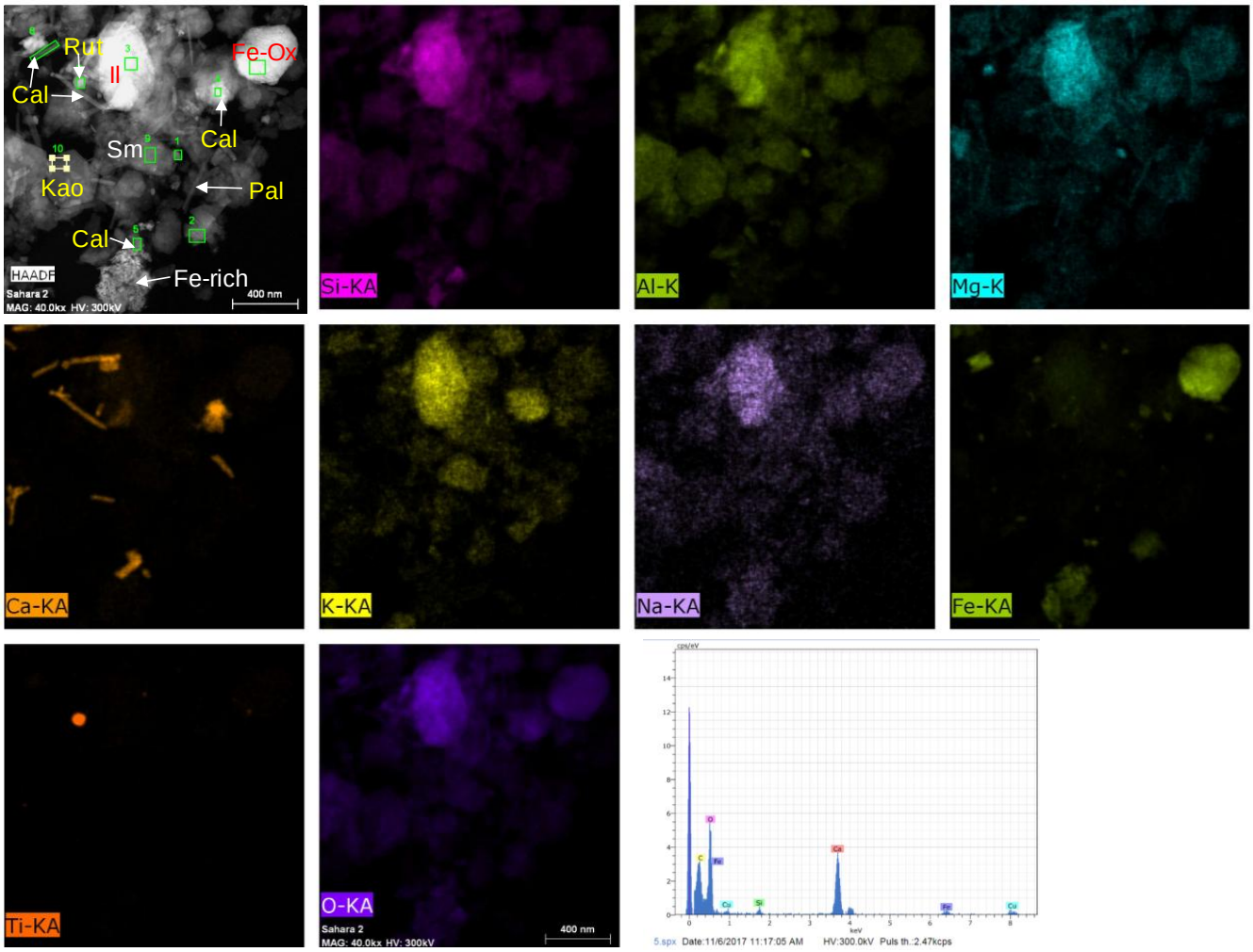


**Figure S5.** STEM-HAADF photomicrographs and corresponding EDX elemental maps of a micrometer-sized aggregate of Saharan dust particles. Based on the compositional analysis, particles of palygorskite (Pal), calcite (Cal), goethite/hematite (Fe-Ox), aggregates of iron oxyhydroxide nanoparticle (Fe-rich), rutile (Rut), illite (Il), smectite (Sm), and kaolinite (Kao) were identified. The EDX spectrum corresponds to calcite in contact with Fe-rich nanoparticles (analysis #5 in HAADF image). Note the absence of S and N. Note: analyzed spots are outlined with green or white (numbered) rectangles in the HAADF image.

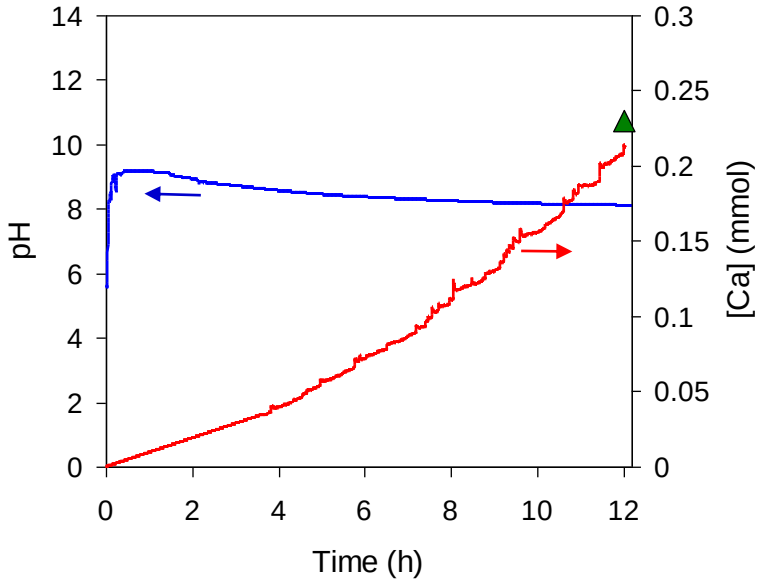


**Figure S6.** Time-evolution of the pH and free calcium concentration [Ca] following dissolution of Saharan dust in MilliQ water with a starting pH of 5.6. The green triangle shows the [Ca] value calculated from PHREEQC modeling.

5

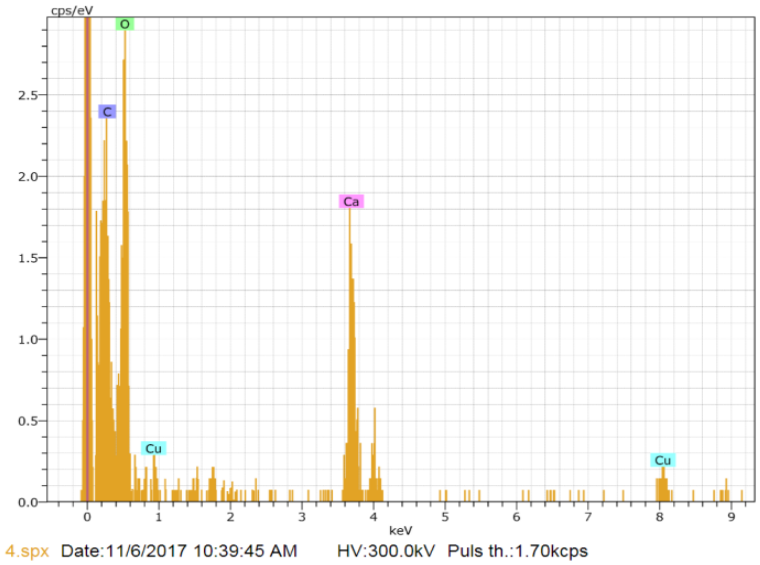


**Figure S7. AEM**-EDX spectrum of an individual calcite grain in Saharan dust (with no sign of Fe contamination by ferrihydrite nanoparticles). Note the absence of Fe in the carbonate (the Cu signal is due to the TEM Cu grid).

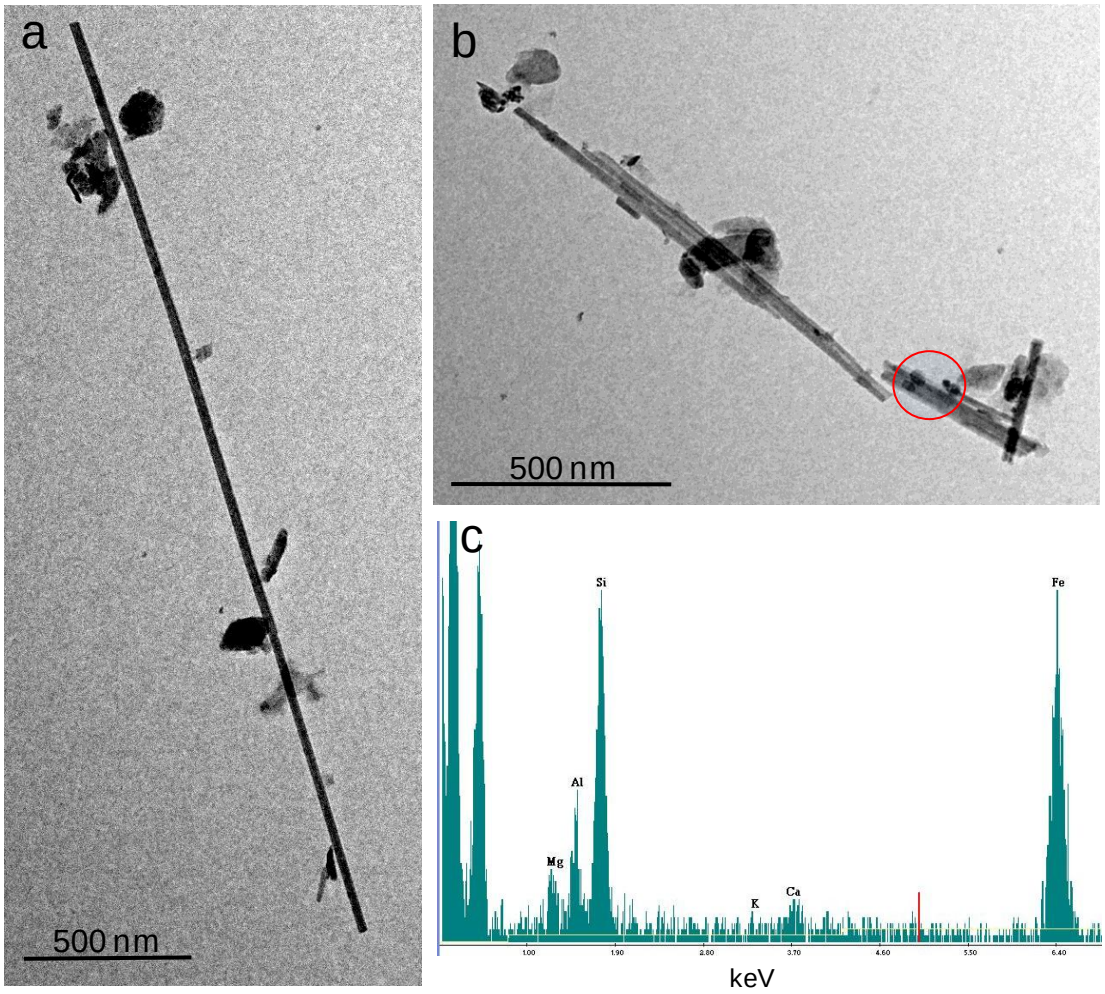


**Figure S8.** TEM photomicrographs and EDX microanalysis of palygorskite fibers in Saharan dust. a) elongated single fiber of palygorskite with attached aluminosilicate particles (feldspars and clay minerals); b) Palygorskite fibers. The red circle points to Fe-rich (dark) nanoparticles attached to the palygorskite fibers; c) EDX spectrum of the Fe-rich nanoparticles in the circled area of (b). The Mg, Al, and Si (along with small amounts of Ca) correspond to the palygoskite substrate,